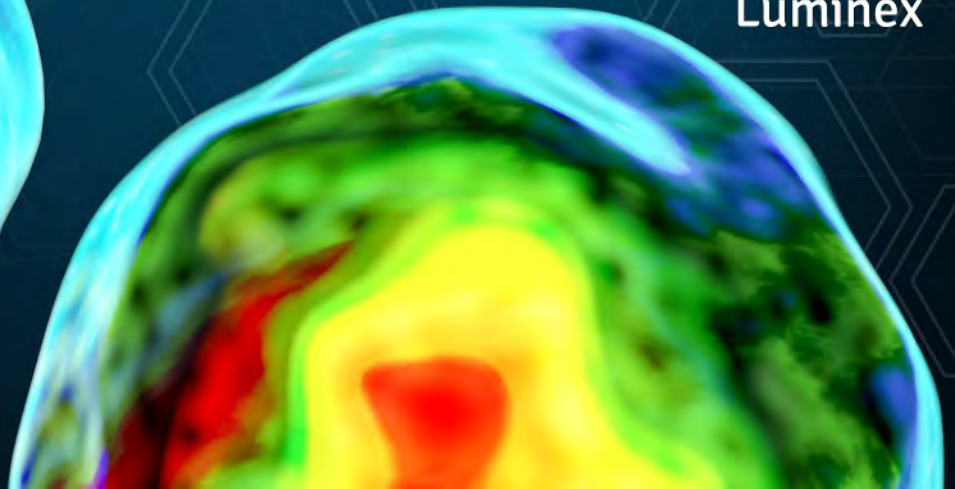
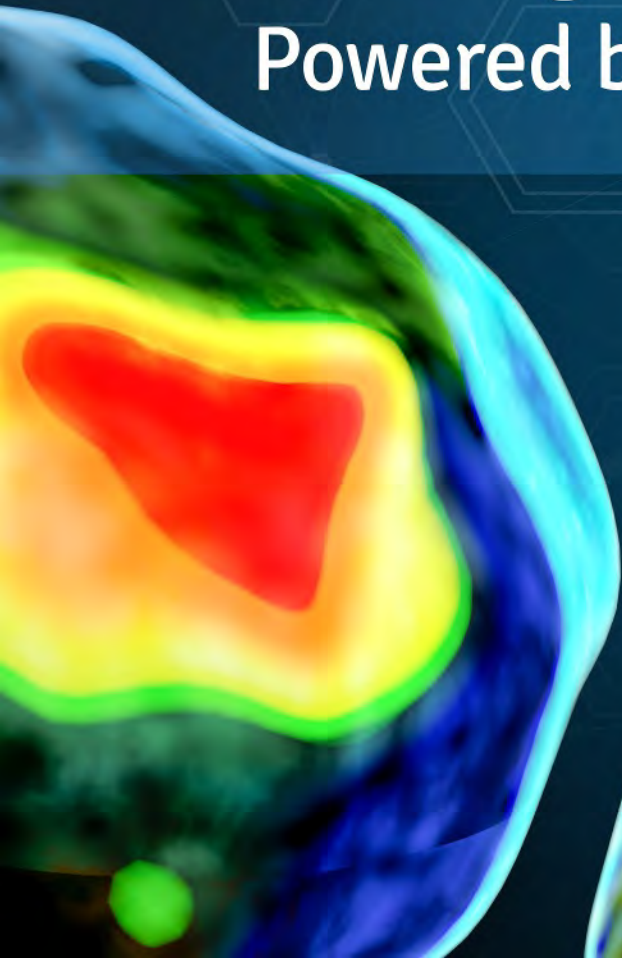


Techniques in Imaging Flow Cytometry Analysis Powered by Artificial Intelligence



 **Biocompare**
The Buyer's Guide for Life Scientists

SPONSORED BY
Luminex

Contents

4 Improved Data Analysis Makes Imaging Flow Cytometry More Accessible

Machine learning and artificial intelligence are being used to help researchers analyze their data more effectively.

7 Automated Scoring of the Micronucleus Assay Using Imaging Flow Cytometry and Amnis® AI

Deep learning improves the detection of subtle image morphologies in the micronucleus assay and permits automated, unassisted scoring.

12 Analysis of T Cell-APC Interactions

Performed using the high-throughput Amnis® FlowSight® Imaging Flow Cytometer and Amnis® AI Image Analysis Software.

16 Morphological Characterization of WBC Five-Part Differential Using Machine Learning

Machine learning enables the characterization of subtle image morphologies to detect multiple populations in white blood cells without the need for immunofluorescence.

22 Resources

Amnis[®]

ImageStream[®]X Mk II and FlowSight[®] Imaging Flow Cytometers



Flow cytometry with vision.

- Imaging in flow enables novel applications.
- Unmatched fluorescence sensitivity detects dim and small particles.
- High-throughput microscopy for robust cell function analysis.

Luminex[®]
complexity simplified.

luminexcorp.com

For Research Use Only. Not for use in diagnostic procedures.

©2020 Amnis, ImageStream, and FlowSight are trademarks of Luminex Corporation, registered in the US and other countries.

For more information, please visit:
luminexcorp.com/imagestreamx-mk-ii/
luminexcorp.com/flowsight-imaging/.

DIGI274495

Improved Data Analysis Makes Imaging Flow Cytometry More Accessible

Machine learning and artificial intelligence are being used to help researchers analyze their data more effectively.

Emma Easthope

For decades, flow cytometry has been recognized as the classic technique for single-cell analysis. Used to detect and characterize distinct—and often incredibly rare—cell types within large, heterogeneous populations, it has seen widespread use to support a diverse range of research applications. However, despite being an extremely fast, sensitive, and quantitative approach to cellular identification, a major limitation of flow cytometry is that it provides no morphological or spatial resolution. This restricts its utility to intensity-based analysis, leaving researchers in the dark when it comes to establishing exactly where in a cell a particular signal originates from.

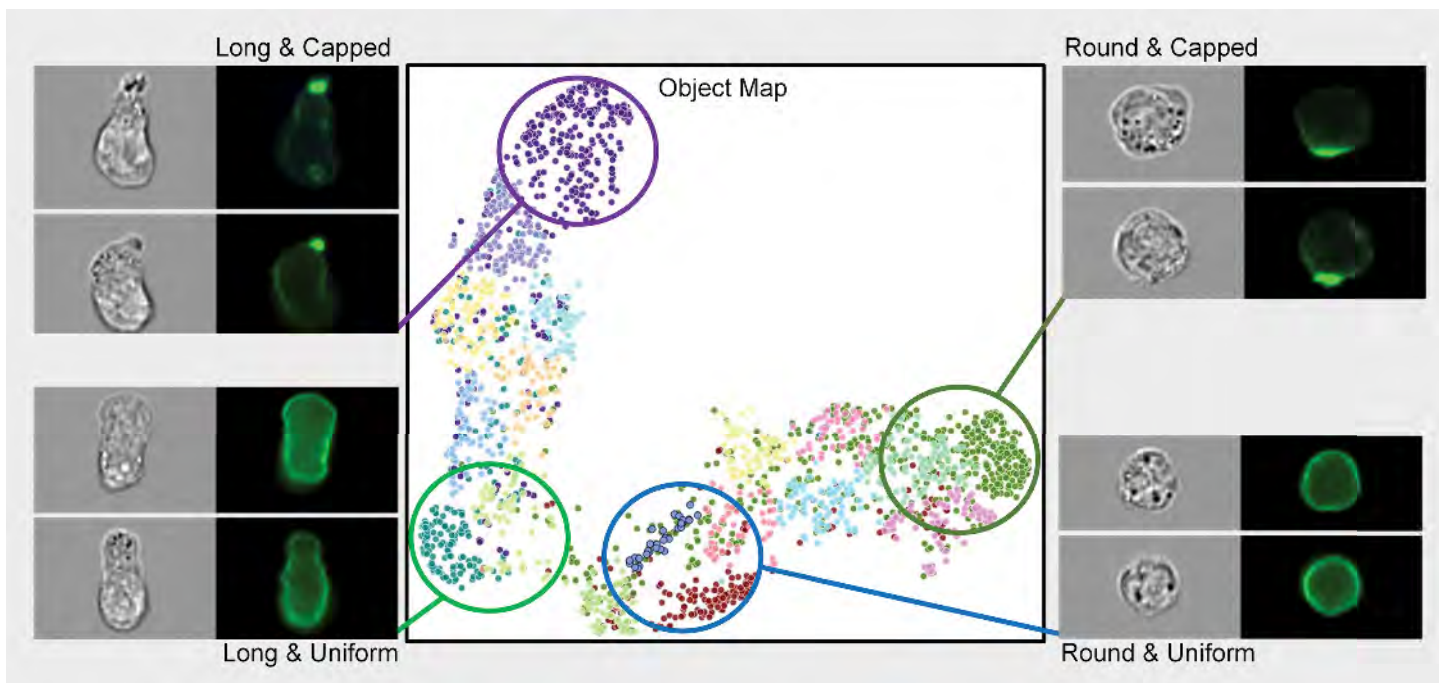
To gain deeper insights from samples that are often available in only short supply, many researchers are turning to imaging flow cytometry (IFC) as a preferred alternative to standard flow cytometry techniques. By combining the high-throughput, multiparametric analysis capabilities and statistical significance of flow cytometry with the morphological and spatial resolution of microscopy, imaging flow cytometry provides researchers with the ability to capture multiple digital images of many thou-

sands of individual cells in just minutes. This information can be used to create highly detailed cellular profiles, allowing comparison with other cell types to interrogate specific sub-populations or to establish links between cellular phenotype and disease.

One of the current challenges of analyzing the vast data sets generated by imaging flow cytometry is the level of expertise necessary to perform complex masking and feature calculation. In this ebook, we explain how leveraging the power of machine learning (ML) and artificial intelligence (AI) can help researchers more effectively analyze their imaging flow cytometry data, before delving into some specific use cases. These include using AI to support micronuclei detection and to measure the immunological synapse and applying machine learning to quantify white blood cells (WBCs).

Benefits of imaging flow cytometry

Unlike conventional flow cytometry, which typically uses fluorescence intensity as a measure of distinct



An object map is a two-dimensional representation of a high dimensional data set, where each color represents a unique population and the proximity between clusters represent how morphologically distinct each population is. In this example, it was used to discover four unique cell populations by viewing images from each cluster. These populations were characterized as long cells with uniform fluorescence, long cells with bright caps, round cells with bright caps and round cells with uniform fluorescence.

cell surface markers, imaging flow cytometry combines brightfield, darkfield, and fluorescence-based detection all in one platform. This is achieved using 20×, 40×, or 60× objectives in addition to a unique time delay integration (TDI) charge-coupled device (CCD) camera. Although both techniques operate similarly, imaging flow cytometry not only acquires fluorescence intensity but also provides detailed imagery of every cell within a sample. To view morphological and structural cellular properties, researchers simply select any dot within a dot plot to look more closely at an individual cell or select a specific bin within a histogram to see all the cells within a defined sub-population.

Depending on the number of fluorescent channels the imaging flow cytometer has available, it

is possible to capture as many as 12 digital images of each cell (brightfield and darkfield images, plus 10 fluorescent readouts), translating to hundreds of thousands of images per sample. The depth of information on a cell-by-cell basis is comparable to that of standard microscopy. However, because imaging flow cytometry also benefits from the statistical significance of large sample sizes common to conventional flow cytometry, it is considerably more powerful than either technique used alone. These features of imaging flow cytometry make it well-suited to a broad range of applications, including studies designed to monitor multiple sub-cellular compartments, or to locate and quantify the distribution of signaling molecules on, in, or between cells.

Challenges of imaging flow cytometry

Although imaging flow cytometry provides extraordinarily rich morphological and spatial information, handling such vast quantities of data presents significant challenges. For want of a better approach, analyses are often based on just a small number of selected features, many of which are identified manually by applying binary gates. While such a strategy can work in the hands of a researcher experienced in imaging flow cytometry analysis, it is highly prone to user bias and requires considerable interaction with the data. Moreover, by failing to consider all the available information, manual analysis of imaging flow cytometry data can lead to valuable insights being overlooked.

New frontiers in analyzing IFC data

Recently, artificial intelligence, and specifically machine learning, have driven huge advances within the field of bioimaging research. Machine learning uses algorithms to identify and separate distinct cellular populations. An example is the linear discriminant analysis (LDA) that creates unique classifiers based on optimally combining multiple image characteristics and morphologies into population-specific features. AI, which utilizes deep learning algorithms, exploits the opportunities afforded by user guided training and computer vision to further simplify multimodal image analysis, thereby reducing user-related variability and improving the overall quality and reliability of imaging flow cytometry data analysis.

As well as helping to reveal findings that would otherwise remain hidden within an overwhelming wealth of experimental readouts, machine learning

and AI have been fundamental in increasing the uptake of imaging flow cytometry. In turn, this has paved the way to the development of novel experimental capabilities, consequently opening up a greater diversity of applications. Areas where imaging flow cytometry has proven especially valuable include phenotyping and identifying circulating tumor cells, studying cell-cell interactions, and monitoring disruptions to cell signaling mechanisms.

To make imaging flow cytometry more accessible, Luminex offers two imaging flow cytometers (the Amnis® ImageStream®X Mk II and the Amnis® FlowSight®) as well as two different software options (IDEAS® 6.3 plus Machine Learning and the Amnis® AI Image Analysis Software, both of which are compatible with either instrument). We will now consider some specific cases where the Amnis® platforms have been deployed: the adaptation of a cytokinesis-block micronucleus (CBMN) assay to an imaging flow cytometry format for improved throughput; measurement of the immunological synapse (a rare entity that has historically been difficult to analyze objectively), using FlowSight® imagery for immunological synapse identification; and development of a method for faster, more accurate quantification of WBCs.

About the author

Emma Easthope is the founder and director of Cambridge Technical Content Ltd, based in the U.K. Since graduating with a bachelor's degree in biology from the University of Kent at Canterbury in 2000, she has gained extensive experience developing and running immunoassays within companies including Millennium Pharmaceuticals, AstraZeneca, and Cellzome.

Automated Scoring of the Micronucleus Assay Using Imaging Flow Cytometry and Amnis[®] AI

Deep learning improves the detection of subtle image morphologies in the micronucleus assay and permits automated, unassisted scoring.

Matthew A. Rodrigues, Ph.D., Christine E. Probst, Bryan Davidson, Michael Riedel, Yang Li, and Vidya Venkatachalam, Ph.D.

Introduction

The micronucleus (MN) assay is required by a number of regulatory bodies as a genetic toxicity screening test. MN originate from whole chromosomes or chromosome fragments that fail to be incorporated into the main nucleus following nuclear division.¹ Consequently, DNA damage can be assessed by quantifying MN in mononucleated (MONO) cells, or in once-divided binucleated (BN) cells through the use of Cytochalasin-B (Cyt-B) to block cellular division—the latter method is preferable.² Additionally, cytotoxicity is typically quantified by scoring the frequency of cells with one, two, and three or more (MULTI) nuclei (Figure 1). As a result, a rigorous set of criteria with which to score the assay has been developed, largely focused on morphological characteristics of the cytoplasmic and nuclear imagery.³

The assay is scored primarily using microscopy—the gold standard—and conventional flow cytometry, each with advantages and limitations. Manual mi-

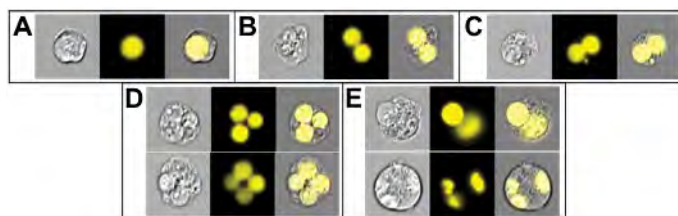


Figure 1. Representative IFC imagery of key events in the cytokinesis-block version of the MN assay. (A) Mononucleated cell. (B) Binucleated (BN) cell. (C) BN cell with a MN. (D) Multinucleated cells. (E) Examples of imagery that should not be scored, including a BN cell with one irregularly shaped nucleus (top) and a multinucleated cell with abnormal nuclear morphology (bottom).

croscopy benefits from high-resolution imaging of nuclear and cytoplasmic cellular components, but is tedious and prone to scorer variability.⁴ Flow cytometry offers high-throughput data acquisition, but lacks the ability to visually confirm key events, making adherence to the scoring criteria impossible.⁵ The use of imaging flow cytometry (IFC) to perform the MN assay overcomes many of the disadvantages of other scoring methods, permitting the high-throughput capture of cytoplasmic and nuclear imagery, as well as

the automated identification and quantification of all key events in IDEAS® Software.⁶ However, IFC requires expert knowledge to create a feature-based analysis strategy in IDEAS that correctly identifies subtle morphologies in the imagery, which can be challenging. Therefore, a more robust and readily accessible image-based solution is desirable.

The Amnis® AI software package is a convolutional neural network (CNN)-based deep learning platform. CNNs are effective at extracting large amounts of information from complex data sets,⁷ and have been shown to be well-suited to analyze IFC data.⁸ There are several advantages to using CNNs to perform the required image analysis in the MN assay, including enhanced translatability across cell lines and the elimination of complex image analysis strategies. Additionally, the Amnis® AI software has been designed with an interface that allows users to interact with the imagery and the neural network in an iterative manner to construct models from their IFC data. This permits users with any level of familiarity with CNNs to train, visualize, validate, and share models.

Here, we describe the use of Amnis® AI software to develop a classification model that scores all critical events in the MN assay and eliminates events that deviate from the scoring criteria. Our results demonstrate that AI-based scoring compares well to manual microscopy, and establishes the feasibility of combining IFC and AI to perform the MN assay.

Materials and methods

Cell culture, exposure to test chemicals, and sample preparation

TK6 cells were cultured (37°C, 5% CO₂) in RPMI-1640 media supplemented with 10% FBS, 1% non-essential amino acids, 1% sodium pyruvate, and 1% penicillin-streptomycin. Test chemicals included Mitomycin C, Etoposide, and Mannitol (negative control),

and were introduced into separate T25 culture flasks containing TK6 cells at approximately 7x10⁵ cells/mL. Following a 3-hour exposure time, cells were centrifuged to remove the test chemical and were cultured in 10 mL of fresh media containing 3 µg/mL of Cytochalasin B (to block cytokinesis) for an additional 24 hours. All samples were then pelleted, and 75 mM KCl was added to swell the cells plus 4% formalin to fix them. Cells were then washed (1X PBS with 2% FBS), stained with Hoechst 33342, and prepared for microscope scoring or IFC data acquisition.

Microscope scoring and IFC acquisition

Using a Nikon Eclipse E600 fluorescent microscope (Nikon, NY, USA), 1,000 BN cells per culture were scored at 100X for the presence of MN to assess genotoxicity, and an additional 500 cells were scored and classified as either MONO, BN, or polynucleated (POLY) cells to assess cytotoxicity.⁹ For IFC data acquisition, all samples were run on an ImageStream®x Mk II dual CCD camera system (Luminex Corporation, Seattle, WA, USA) at 40X magnification with the 405 nm laser set to 15 mW. Channels 1 and 9 were used to capture cytoplasmic images from the BF LED and Hoechst images (nuclei and MN) were captured in channel 7. All MMC samples were loaded manually and three data files of 15,000 events per culture were collected. All Etoposide and Mannitol samples were acquired using the 96-well plate autosampler and 30,000 events were collected per culture. The statistical significance of any increase in the number of micronucleated cells was evaluated using a one-sided Fisher exact test (p < 0.001).

Results

Model development in the Amnis® AI software package

The Amnis® Alsoftware (v1.0) trains machine learning models based on ground truth input data and applies these models to classify new data. The con-

volutional neural network (CNN) is designed to work optimally on image data acquired on Amnis® IFCs. Using Amnis® AI software, a model was built and trained to score all key events in both versions of the MN assay,¹⁰ though only results relevant to the cytokinesis-block version will be discussed in this article. A total of 25 data files from the MMC experiments were loaded into the Amnis® AI software. Ground truth model classes representing the key imagery to be scored were created and populated using the cluster and predict algorithms. Using segments of 1,500 images randomly selected by the software, the cluster algorithm groups similar objects together. As the ground truth model classes become more well-defined, the clustering improves and islands of like-imagery within a segment begin to emerge (Figure 2A). The predict algorithm assigns model classes to the remaining unclassified objects based on the imagery of the ground truth data. Since the predict algorithm assigns classes to objects that are unlike the cluster algorithm, it requires at least 25 examples of each class. Generally, providing more examples of ground truth will improve the results of the predict algorithm and the quality of the visualization on the object map (Figure 2). The advantage of this workflow is that from within the cluster or predict algorithms, the user can assign individual objects, entire clusters, or whole predicted groups to the appropriate ground truth model classes, enabling rapid construction of models containing thousands of ground truth objects. A total of 31,500 ground truth objects were split into an 80/10/10 ratio to train, validate, and then test the model.

Amnis® AI MN model accuracy

Table 1 shows the accuracy of the model to score all the relevant key events in the cytokinesis-block version of the MN assay. Amnis® AI software provides results for precision, recall, and F1—common AI metrics to measure model accuracy in machine learning. Pre-

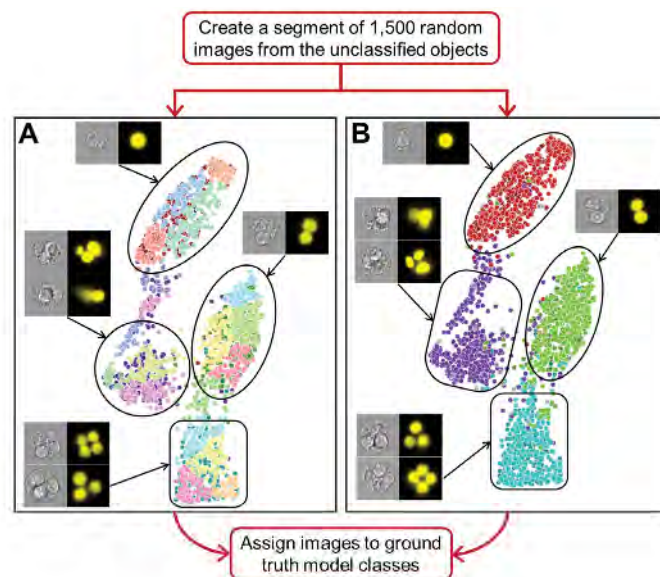


Figure 2. Diagrammatic view of the Amnis® AI software workflow. Once the user has loaded data into the Amnis® AI software, the segment option is used to randomly select 1,500 objects. The user can run the cluster algorithm (A), which the software uses to group like objects together based on the imagery of both the unclassified and the ground truth objects. The predict algorithm (B) can also be run, which attempts to predict the correct model classes for all unclassified objects in the segment based on learning from the truth objects already assigned to specific classes. From the results of both the cluster and predict algorithms, the user then manually assigns objects (individually or in large groups) to their appropriate ground truth model classes.

Table 1. Precision, recall, and F1 scores for the relevant model classes for the cytokinesis-block version of the MN assay. Accuracy statistics ranged from 85.1% to 99.0% for all classes.

Model class	Precision (%)	Recall (%)	F1 score (%)
Mononucleated cell	97.0	99.0	98.0
Binucleated cell	98.8	97.4	98.1
Binucleated cell with MN	95.0	97.7	96.3
Multinucleated cell	93.7	97.8	95.7
Irregular morphology	91.6	85.1	88.3

cision and recall individually provide a measure of the rate of false positives and false negatives, respectively.

The F1 score is the harmonic mean of precision and recall, and provides a broader view of the overall accuracy of the model. The model accuracy statistics ranged from 85.1% to 99.0%, with the lowest accuracy occurring in the irregular morphology class. This is not unexpected, as many objects that belong in this class have subtle morphological irregularities in the imagery (e.g., slightly overlapping nuclei, nuclei of different sizes and/or intensities, etc.), which necessitate their exclusion from scoring.³ In general, the model performs well to identify all key events in the cytokinesis-block version of the MN assay.

Microscopy and Amnis® AI dose-response data

Figure 3 presents the dose-response results following exposure of TK6 cells to Mitomycin C, Etoposide, and Mannitol for both microscope and Amnis® AI scoring. For MMC and Etoposide, statistically significant increases ($p < 0.001$) in the number of micronucleated cells were observed in all doses tested when compared to solvent controls. For Mannitol, no statistically significant increases in MN frequency were observed at any dose, as expected. Cytotoxicity values were higher for Amnis® AI scoring than for microscopy, which may be the result of improved robustness of the assay when using IFC, as many more cells can be scored. On average, across all data files, 5,500 MONO cells, 7,200 BN cells, and 1,300 POLY cells were scored—a total of 14,000 cells. This represents a substantial increase in the number of cells typically scored for the presence of MN and to assess cytotoxicity, respectively.⁹

Conclusions

This article demonstrates the use of the Amnis® AI software package to identify and quantify key imagery in the MN assay. The use of IFC combined with an image-driven CNN analysis model offers a number

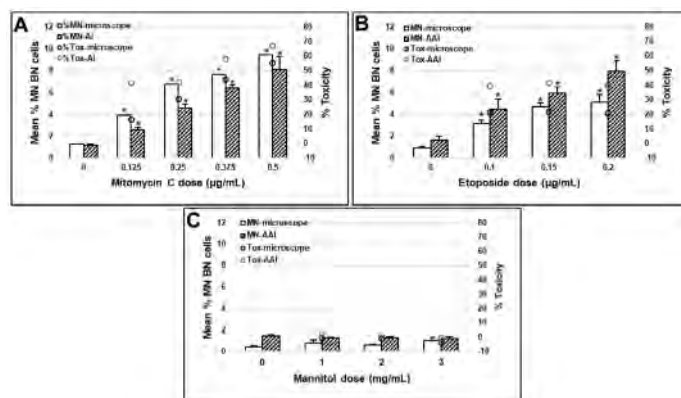


Figure 3. Genotoxicity measured by the percentage of BN cells with MN using microscopy (clear bars) and Amnis® AI (striped bars), as well as cytotoxicity assessed by microscopy (black circles) and Amnis® AI (blue circles) for (A) Mitomycin C (MMC), (B) Etoposide, and (C) Mannitol. Asterisks indicate statistically significant increases in MN frequency. Error bars represent the standard error of the mean (SEM) of the MN frequency from six data file replicates (three data files per culture from duplicate cultures) for MMC, and the SEM of MN frequency from one data file per culture from triplicate cultures for Etoposide and Mannitol.

of advantages over traditional scoring methods, including a dramatically simplified analysis workflow and higher translatability due to the plasticity of the neural network in comparison to feature-based image analysis techniques. Additionally, through the combination of IFC and Amnis® AI, several thousand more key events can be scored than is feasible with microscopy, providing a more statistically robust quantification of genotoxicity and cytotoxicity. Furthermore, the use of Amnis® AI to score the MN assay is more streamlined, as it overcomes the tedious nature of microscope scoring and eliminates the complexities of feature-based image analysis. Furthermore, with the availability of several additional image detection channels on the CCD camera, a multiplex assay could be developed in which markers are included for the identification and quantification of apoptotic and necrotic cells that would also have the potential to incorporate nuclear membrane

markers to further confirm the legitimacy of MN via colocalization with the DNA stain.

Overall, the results presented here demonstrate how the use of an Amnis® AI model to score the MN assay yields results that are comparable to visual microscopy—the gold standard scoring method—and offers several advantages over both microscope, and flow cytometry-based methods.

About the authors

All authors are employees of Luminex Corporation. Matthew A. Rodrigues is a Field Applications Scientist, Christine E. Probst is a Senior Scientist, Bryan Davidson is a Senior Algorithm Scientist, Michael Riedel is a Senior Software Engineer, Yang Li is a Senior Algorithm Scientist, and Vidya Venkatachalam is a Senior Director of Software and Algorithms R&D.

References

1. Fenech M, et al. HUMN project initiative and review of validation, quality control and prospects for further development of automated micronucleus assays using image cytometry systems. *Int J Hyg Env Health*. 2013. 216, 541–52.
2. Fenech M. Commentary on the SFTG international collaborative study on the in vitro micronucleus test: to Cyt-B or not to Cyt-B? *Mutat Res*. 2006. 607, 9–12.
3. Fenech M, et al. HUMN project: Detailed description of the scoring criteria for the cytokinesis-block micronucleus assay using isolated human lymphocyte cultures. *Mutat Res - Genet Toxicol Environ Mutagen*. 2003. 534, 65–75.
4. Fenech M, et al. Intra- and inter-laboratory variation in the scoring of micronuclei and nucleoplasmic bridges in binucleated human lymphocytes: Results of an international slide-scoring exercise by the HUMN project. *Mutat Res Toxicol Environ Mutagen*. 2003. 534, 45–64.
5. Bryce SM, Bemis JC, Avlasevich SL, and Dertinger SD. In vitro micronucleus assay scored by flow cytometry provides a comprehensive evaluation of cytogenetic damage and cytotoxicity. *Mutat Res Toxicol Environ Mutagen*. 2007. 630, 78–91 (6).
6. Rodrigues MA. Automation of the in vitro micronucleus assay using the Imagestream® imaging flow cytometer. *Cytometry A*. 2018. 93, 706–726.
7. LeCun Y, Bengio Y, and Hinton G. Deep learning. *Nature*. 2015. 521, 436–444.
8. Probst C, Zayats A, Venkatachalam V, and Davidson B. Advanced Characterization of Silicone Oil Droplets in Protein Therapeutics Using Artificial Intelligence Analysis of Imaging Flow Cytometry Data. *J Pharm Sci*. 2020. doi: 10.1016/j.xphs.2020.07.008. [https://jpharmsci.org/article/S0022-3549\(20\)30371-3/fulltext](https://jpharmsci.org/article/S0022-3549(20)30371-3/fulltext)
9. OECD Library. Test No. 487: In Vitro Mammalian Cell Micronucleus Test. *OECD Guidel Test Chem. Sect. 4*. 2016. doi.org/10.1787/20745788.
10. Rodrigues MA, et al. The in vitro MN assay by imaging flow cytometry and deep learning. *Nat Commun*. 2020. (Submitted.)

For Research Use Only. Not for use in diagnostic procedures.

Amnis and ImageStream are trademarks of Luminex Corporation, registered in the U.S. and other countries.

Analysis of T Cell-APC Interactions

Performed using the high-throughput Amnis® FlowSight® Imaging Flow Cytometer and Amnis® AI Image Analysis Software.

Maria Gracia Garcia Mendoza, Ph.D., Bryan Davidson, and Haley R. Pugsley, Ph.D.

T cells are activated through the interaction of the antigen-specific T cell receptor (TCR)-CD3 complex and major histocompatibility complexes (MHCs) on the surface of an antigen-presenting cell (APC). These interactions result in signaling transduction pathways that lead to the proliferation and differentiation of T cells, permitting proper immune responses.^{1,2}

The immune synapse (IS) is a dynamic and highly organized interface between a T cell and an APC. IS formation requires cortical actin cytoskeleton rearrangement, which provides stability when receptors bind to F-actin bundles.^{3,4} IS formation can be measured using fluorescence microscopy (e.g., confocal, TIRF, or super-resolution techniques) by fluorescently labeling molecules that are recruited to the interface and imaging their colocalization. However, immune synapses are rare events, and studying them using traditional microscopy techniques can be difficult, time-consuming, and can generate low statistical significance.

In this study, we used the **Amnis® FlowSight®** Imaging Flow Cytometer and IDEAS® Software to isolate T cell-APC conjugates, identify the region of cell contact by F-actin localization, and evaluate the percentage of T cells with organized immune synapses. Further, we employed Amnis® AI Image Analysis

Software for immune synapse image classification, and included criteria to identify subtle morphological differences, improving the efficacy of the classification model.

Identifying conjugates

To generate T cell-APC conjugates, Raji B cells were treated with 5 µg/mL Staphylococcal enterotoxin B (SEB) to make APCs. T cells were isolated from human blood with RosetteSep™ prep (Stemcell Technologies). T cells and APCs were incubated at a 1:1 ratio for 45 min. After incubation, the cells and conjugates were fixed and stained with CD19-AlexaFluor™ 488, CD3-PE-TexasRed™, Phalloidin (F-actin)-AlexaFluor™ 647, and DAPI.

The FlowSight® Imaging Flow Cytometer with a 20X objective was used to collect 30,000 events.

Figure 1 shows the gating strategy to isolate conjugates using Amnis® IDEAS® Software.

By plotting the Bright Detail Intensity of F-actin vs. the Bright Detail Similarity (colocalization) of CD3 and CD19 at the interface (Figure 1E; Valley mask), we quantified the percentage of T cells in an organized immune synapse. The percentage of T cells in the immune synapse gate was 10.04% for the SEB-treated sample vs. 0.98% for the control (no SEB).

Careful examination of the cells in the “No Synapse” and “Immune Synapse” populations revealed several conjugates that contained more than two cells had slipped through the initial gating strategy (Figure 1F). Identifying these cells for exclusion in IDEAS can be time-consuming with large sample sizes, so we employed the new Amnis AI Image Analysis tool. Image classification in Amnis AI is based on convolutional

neural networks (CNN), a type of deep learning neural network that uses convolution to interpret visual inputs.⁵ Amnis AI works by training a classification model based on truth input data and applying the trained model to classify new data. Data files from five different independent experiments were merged using IDEAS Software. To create the IS Amnis AI model, truth populations (including “No Synapse,” “Immune

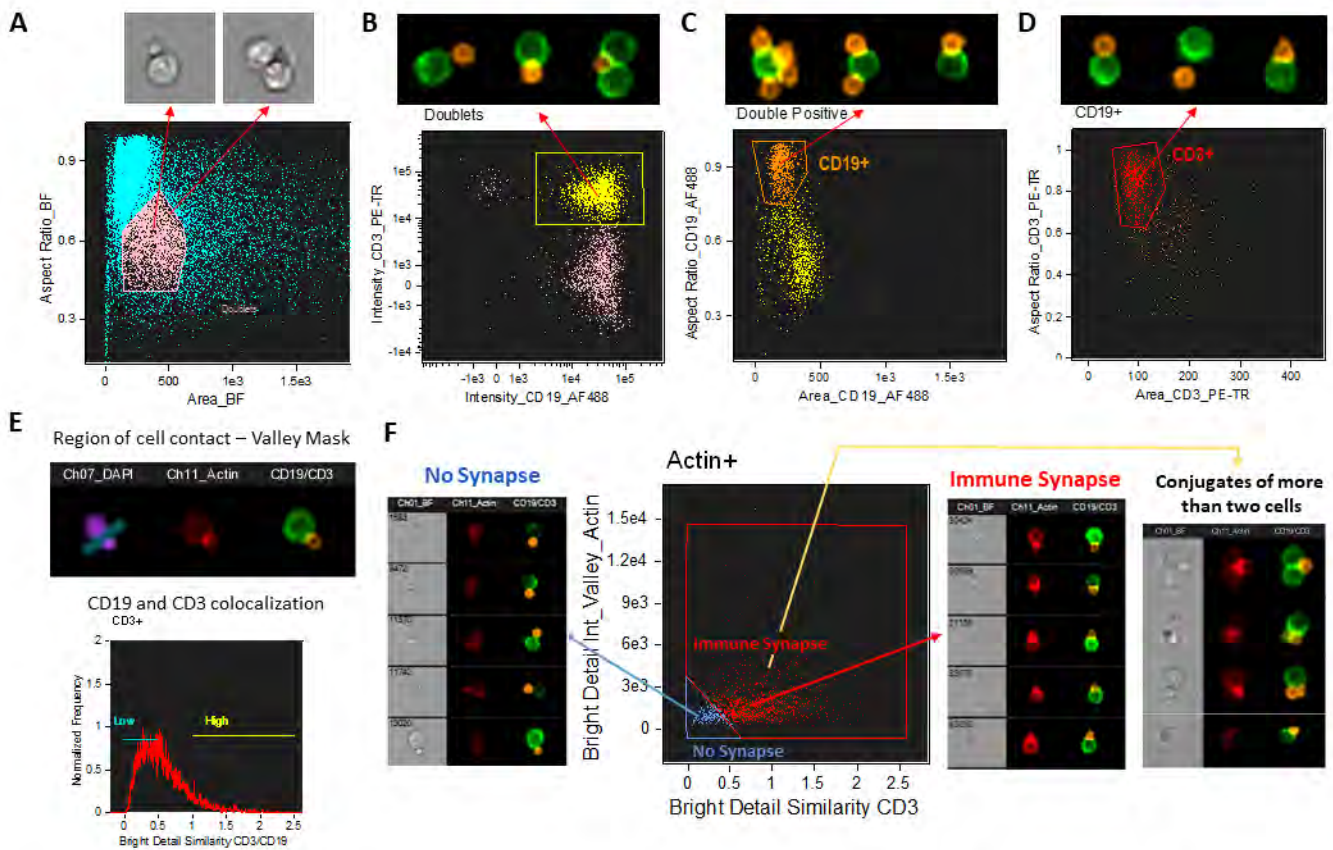


Figure 1. Gating strategy for immune synapses in IDEAS® Software. A) The aspect ratio vs. the area of the Brightfield (BF) image identifies doublets. B) The intensity of CD3 vs. CD19 identifies doublets with both CD3 (orange) and CD19 (green). C) The aspect ratio vs. the area of the CD19 signal from the doublet population identifies doublets with only one CD19+ cell. D) The aspect ratio vs. the area of the CD3 signal from doublets identifies those with only one CD3+ cell. E) A Valley mask applied on DAPI identifies the interface of the synapse, where the two cells connect. The high expression of actin in this region identifies an immune synapse. The Bright Detail Similarity of the CD3 and CD19 signals identifies conjugates that have overlapping CD3 and CD19, indicating a strong junction between the T cell and the APC. F) The Bright Detail Intensity at the interface with high actin signal vs. the Bright Detail Similarity (colocalization) of CD3 and CD19 identify the “No Synapse” and “Immune Synapse” populations. Confirmatory single image analysis by eye identifies conjugates with more than two cells (yellow arrow, Figure 1F).

Synapse,” and “More than 2 Cells”) were imported from IDEAS Software and were hand-tagged. Each population contained approximately 600 conjugates. The input channels included Brightfield (Ch1), CD19 (Ch2), CD3 (Ch4), and Actin (Ch11). A training experiment was created, and the model was trained and applied to the control and SEB-treated samples reported in Figure 1. The DAF files were updated to visualize the classification in IDEAS.

Evaluating the accuracy of the Amnis® AI model

The prediction probability provides an overall indicator of confidence for each population (Figure 2A). The columns represent the objects predicted to be members of the corresponding population; rows show the median prediction probability for each population. Elements on the diagonal represent a match of truth data to prediction, with larger numbers indicating higher confidence.

The classification efficiency of the model (Figure 2B) describes Precision (a measure of false positives where $\text{Precision} = \text{true positive} / (\text{true positive} + \text{false positive})$), Recall (a measure of false negatives where $\text{Recall} = \text{true positive} / (\text{true positive} + \text{false negative})$), and the F1 score (a measure of the accuracy of the model where $\text{F1} = 2 * (\text{Precision} * \text{Recall}) / (\text{Precision} + \text{Recall})$), where larger values indicate higher accuracy. Scores for the Amnis AI model averaged 91%.

Utilizing Amnis AI, the percentage of T cells in the immune synapse gate was 7.01% for the SEB-treated sample vs. 0.65% for the control (no-SEB); this is an accurate count that easily excluded conjugates with more than two cells (as seen in yellow, Figure 2C).

Applying the model to experimental data

The accuracy of the Amnis® AI model was validated by exposing Raji B cells to various concentrations of SEB (0–20 µg/mL) for 15 min to make APCs. Then, T cells were incubated with SEB-treated Raji cells at a 1:1 ratio for 45 min before being fixed and stained as described above. An Amnis AI classification experiment was created using the IS Amnis AI model, and the percentage of T cells with immune synapses was calculated for each SEB concentration in a clas-

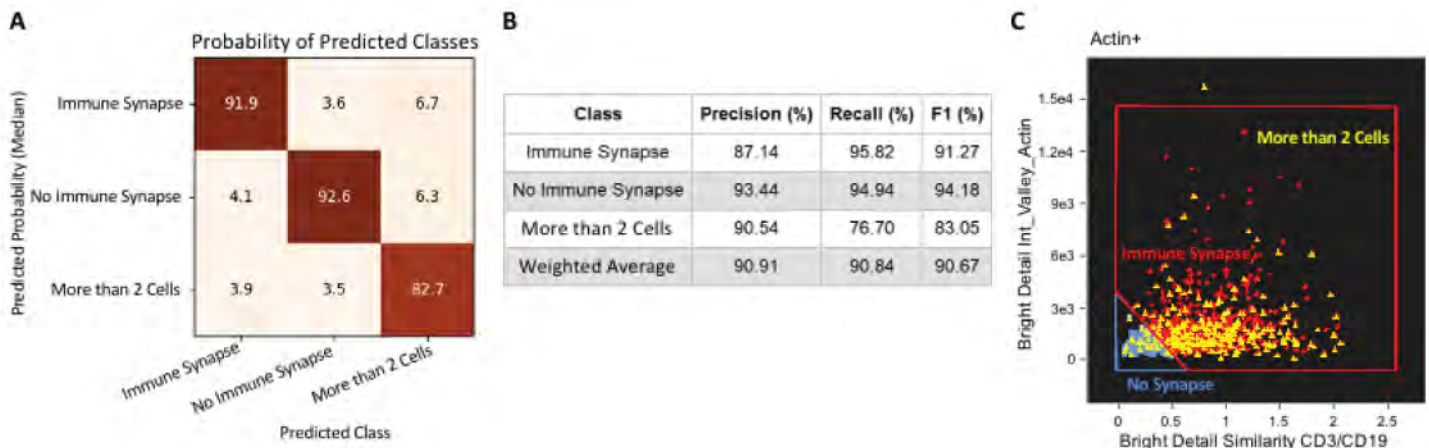


Figure 2. Amnis® AI training experiment results. A) Confusion matrix of truth vs. classification results of the training experiment. B) Classification efficiency of the IS Amnis AI model. C) Updated histogram displaying the conjugates with more than two cells identified by the IS Amnis AI model in yellow.

sification experiment. As expected, the percent of T cells in synapse increased with increasing SEB doses (Figure 3).

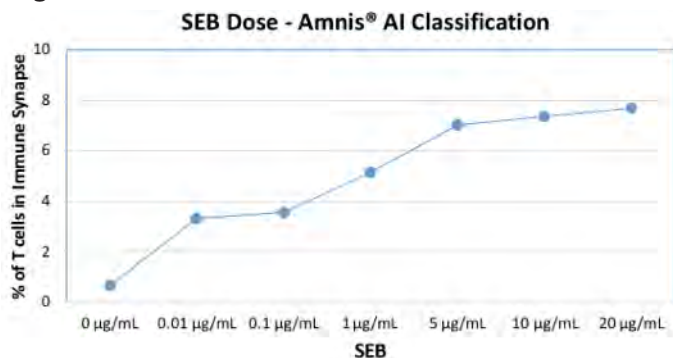


Figure 3. Percentage of T cells in immune synapse after exposure to different doses of SEB.

Conclusions

The quantitative power of large sample sizes and microscopy information provided by FlowSight® imaging flow cytometry can measure the formation of the immunological synapse and actin aggregation at the interface. IDEAS® Software is a powerful tool that provides advanced imaging cytometry analysis techniques; however, to analyze IS, it takes an experienced user to create the appropriate features and masks for the analysis, which can be difficult. In this experiment, conjugates with more than two cells could still be visualized in both the “Immune Synapse” and “No Synapse” populations after time-consuming, image-by-image identification. Using Amnis® AI Image Analysis Software, these conjugates were easily identified, offering a more accurate and reliable method for quantifying rare events such as T cells with immunological synapses. Further, Amnis AI Image Analysis Software partners with IDEAS to greatly simplify data analysis, providing robust imaging classification results that transfer well to similar applications.

Acknowledgments

We would like to thank Dr. Sherree Friend for her help and guidance with the IDEAS analysis.

Amnis, FlowSight, and Ideas are trademarks of Luminex Corporation, and are registered in the U.S. and other countries. Alexa Fluor and Texas Red are trademarks of Thermo Fisher Scientific. RosetteSep is a trademark of STEMCELL Technologies Inc.

About the authors

All authors are employees of Luminex Corporation. Maria Gracia Garcia Mendoza, Ph.D., is a Scientist II, Bryan Davidson is a Senior Algorithm Scientist, and Haley R. Pugsley, Ph.D. is Manager, Senior Scientist.

References

1. Dustin, ML. The immunological synapse. *Cancer Immunol Res.* 2014;2(11):1023-1033.
2. Martin-Cofreces N, Baixauli F, Sanchez-Madrid F. Immune synapse: conductor of orchestrated organelle movement. *Trends Cell Biol.* 2014;24(1):61-72.
3. Wabnitz G, Kirchgessner H, Samstag Y. Qualitative and quantitative analysis of the immune synapse in the human system using imaging flow cytometry. *J Vis Exp.* 2019;(143).
4. Wulfing C, Davis M. A receptor/cytoskeletal movement triggered by costimulation during T cell activation. *Science.* 1998;282(5397):2266-2269.
5. Probst C, Zayats A, Venkatachalam V, et al. Advanced characterization of silicone oil droplets in protein therapeutics using artificial intelligence analysis of imaging flow cytometry data. *J Pharm Sci.* 2020;7.

For Research Use Only. Not for use in diagnostic procedures.

Morphological Characterization of WBC Five-Part Differential Using Machine Learning

Machine learning enables the characterization of subtle image morphologies to detect multiple populations in white blood cells without the need for immunofluorescence.

Vidya Venkatachalam, Ph.D., and Phil Morrissey, Ph.D.

Introduction

A white blood cell (WBC) differential is an enumeration of the counts and relative percentages of specific cell types in blood, and is a critical component for evaluating patient health and detecting the presence of infection or disease. A key component of WBC differential analysis is the five-part differential, which enumerates the eosinophil, neutrophil, basophil, monocyte, and lymphocyte populations. In the absence of disease or illness, each of these five populations should fall within a specific range, so if any of these populations appears outside of these ranges, the sample is flagged for further evaluation.

The WBC differential is typically performed by morphologically assessing between 100 and 200 WBCs on a slide. However, this manual process can lack objectivity, repeatability, and scalability, and makes it difficult to quantify subtle changes or identify less prevalent cell populations. To address the limitations of manual differential assessment, flow cytomet-

ric methods that incorporate immunofluorescence staining to identify specific cell types have been developed and have gained prominence in recent years. These methods involve using several markers to identify and quantify one or more cell types.

Flow cytometric methods offer the benefit of providing objective, repeatable results that scale well; However, they can be expensive and sample preparation may be time-consuming. Furthermore, flow cytometry alone does not provide the image data needed to morphologically assess the validity of the identified populations, which is a significant barrier to their adoption. In this paper, we discuss a solution that uses imaging flow cytometry (IFC) and machine learning (ML) to overcome these shortcomings, while providing the benefits of both manual microscopic imaging and flow cytometric analyses.

There are two key technologies used in our solution—the **Amnis® ImageStream^{®x} Mk II** Imaging Flow Cytometer, which can rapidly acquire thou-

sands of images of spatially aligned cells in different modes, such as Brightfield (BF), side scatter (SSC), and several fluorescent channels, and the accompanying IDEAS® 6.3 image processing and statistical data analysis software, which provides sophisticated analysis tools to characterize cell morphology using shape, size, texture, and signal intensity features. Using mathematical computational methods based on the Linear Discriminant Analysis (LDA) ML algorithm, we convert these multi-dimensional biological input data characteristics into outputs that can be easily conceptualized and used for image classification. By combining rapid acquisition and sophisticated data analysis technologies, the method we present here offers the benefit of being able to rapidly acquire and assess large numbers of cells for statistical robustness, along with ML algorithms for morphological image classification to obtain a readily understandable and acceptable method for reliable verification of cell classification results.

In our cell classification paradigm, the user provides representative images for each of the populations of interest to train the classifier. This can be accomplished by manually identifying example images, or when applicable, using immunofluorescence to objectively identify the specific cell populations used to train the ML classifiers. Allowing the user to provide the training data results in the classifier output being tuned to the specific needs of the underlying application. The tuned classifier can then be directly applied to test data in the same or similar experiments to identify the different populations. This process removes manual subjectivity from the analysis, leading to results that are highly objective, repeatable, statistically significant, and scalable.

Our method has two main components:

Training: Let M = the number of populations the user wants to classify where $M \geq 2$. The user supplies the

M training populations. We start by computing $N = 1,000+$ features per cell based on shape, size, texture, and signal strength, for the whole and specific cell compartments, including the nucleus, cytoplasm, and the membrane, using imaging modalities such as BF, SSC, and fluorescence. Thus, each cell is a point in N -dimensional feature space where $N \gg 1,000$. Next, we identify the features that best discriminate between cells in the different populations using a modification of Fisher's Linear Discriminant criterion. Finally, we linearly combine the identified features based on the LDA ML algorithm after suitably normalizing and weighting them to maximize discrimination. This results in M 1-dim classifier feature definitions, one for each population. Thus, we collapse a multi-parameter space onto a 1-parameter histogram, which can be readily conceptualized and reported.

Application: Given a data sample, we compute the M classifier features using the definitions determined during training for every cell in the data set, and then apply them to identify the M different populations.

This method effectively analyzes multi-parametric data sets by first obtaining the most discriminating features and collating the features identified into a single 'super-feature' classifier, which can then be used to identify the cells in the data set. The method is robust and generalizes well across multiple application domains. In this paper, we discuss the application of this method to the classification of WBCs into five different populations with widely varying prevalence and subtle morphological differences.

Methods

Data acquisition and generation of training and validation data

Image files were acquired in flow using the Amnis® ImageStream®^{MX} Mk II Imaging Flow Cytometer. Sin-

gle-color controls were used to calculate a spectral crosstalk matrix that was applied to the image files in order to isolate probed images into single imaging channels. Figure 1 shows the five-part panel designed to identify the eosinophil, neutrophil, basophil, monocyte, and lymphocyte populations to use for training and validation of the classifiers, as well as the test panel that contained only the nuclear dye Hoechst, in addition to the BF and SSC channels. Figure 2 shows the gating scheme used to obtain the training and validation data for each of these 5 populations.

The compensated image files were analyzed using image-based algorithms and the ML module in the IDEAS® 6.3 image processing and statistical analysis software package. While information from the fluorescent markers was used to identify the five popu-

	Ch01	Ch02	Ch03	Ch05	Ch06	Ch07	Ch11
Panel 5-Part	BF	CD14- AF488	CD193- PE	CD123- PECy5	SSC	Hoechst	CD45- AF647
Panel Test	BF				SSC	Hoechst	

Figure 1. Panels used for obtaining training data (Panel 5-Part) and test data (Panel Test).

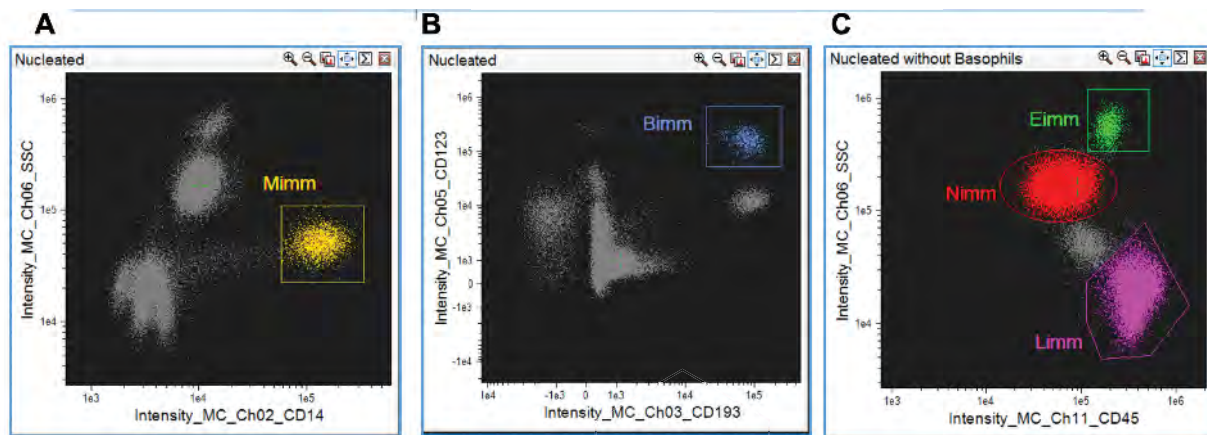


Figure 2. Gating scheme to identify the populations for the WBC 5-part differential using immunofluorescence to use for training and validation. First, the single, focused, and nucleated cells are identified. From the nucleated cells, the monocytes (Mimm) are identified as CD14+ (A) and basophils (Bimm) as CD193+/CD123+ (B). Then, the eosinophils (Eimm), neutrophils (Nimm), and lymphocytes (Limm) are identified from the CD45 vs SSC plot (C).

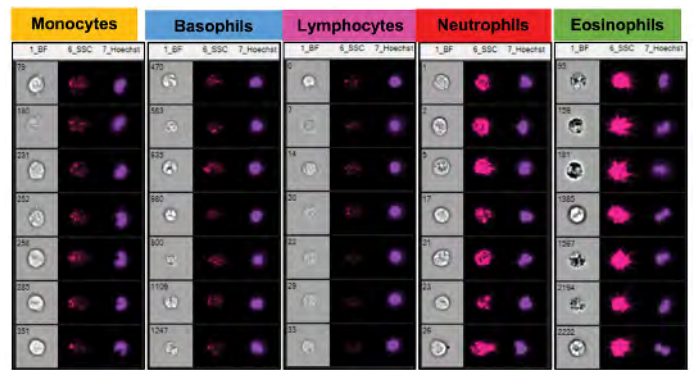


Figure 3. Representative imagery from the BF, SSC, and Hoechst channels used to train the Machine Learning (ML) classifiers.

lations for training and validation, only the BF, SSC, and Hoechst channels were used to generate the classifiers using the ML module. Representative imagery from the BF, SSC, and nuclear (Hoechst) channels of each of these identified populations is shown in Figure 3.

Creating ML classifiers

Careful examination of the images shown in Figure 3 for the five classes reveals that the different classes exhibit variations in nuclear shape and size, SSC

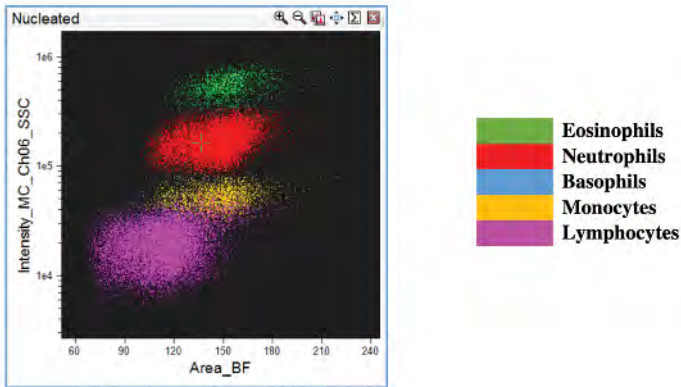


Figure 4. Plot of BF Area vs. SSC Intensity that demonstrates clear separation of the eosinophil and neutrophil populations, unlike the basophil, monocyte, and lymphocyte populations, which are far more difficult to tell apart.

intensity, and BF texture and size. Furthermore, the eosinophil and neutrophil populations can be readily separated using a combination of BF area and SSC intensity, as shown in Figure 4. We used this information to design ML classifiers that could separate all five populations robustly and optimally.

The LDA-based classification methodology used in the ML module is illustrated in Figure 5.

Our classification strategy using this module was as follows:

- Create training sets of about 500 objects each for the lymphocyte, monocyte, and basophil populations. To account for sample and instrument variations, we included data from five donors acquired on two different instruments.
- Create ML classifiers for the basophil and lymphocyte populations using *Bimm* and *Limm* as input training data for the ML module.
- Create ML classifiers for the monocyte and lymphocyte populations using *Mimm* and *Limm* as input training data for the ML module.

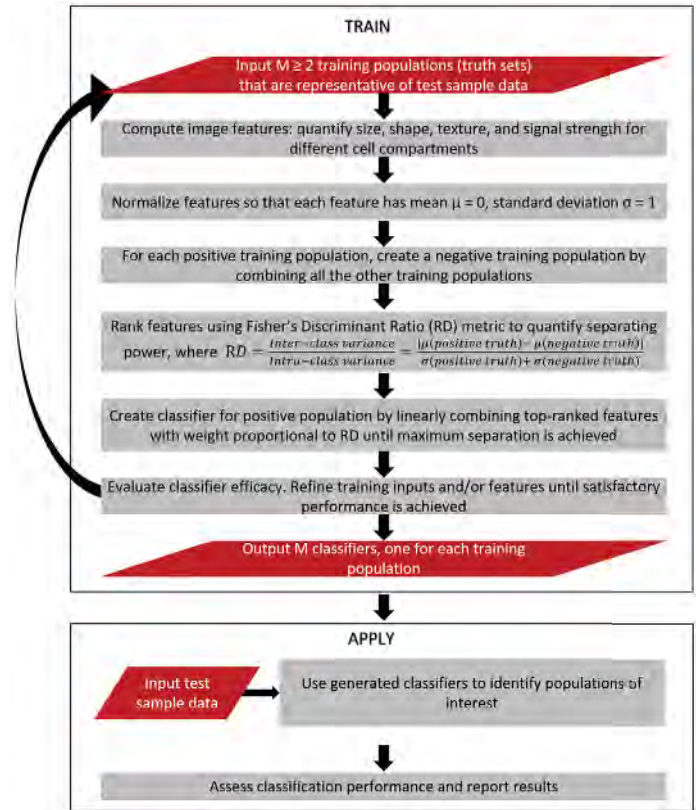


Figure 5. Multi-parameter data classification methodology using Linear Discriminant Analysis in the IDEAS® 6.3 ML module.

- Using the generated ML classifiers from b and c, set up the gating scheme to identify the five populations, as shown in Figure 6.

Results

The classification strategy to identify all five WBC populations using the basophil and the monocyte ML classifiers had excellent qualitative concordance with immunofluorescence, as shown in Figure 6. To quantify the degree of concordance, we computed the sensitivity and specificity metrics, which are defined in Figure 7. Both metrics were well over 95% for all five populations.

Once the classification strategy was finalized, we performed a comprehensive evaluation of the ML

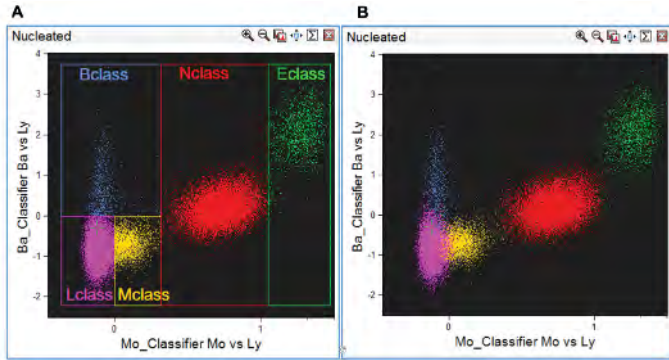


Figure 6. Gating scheme to identify the five populations using the ML classifiers. An important attribute of the classifiers generated by the ML module is that the classifier is positive for the associated population. We leverage this property to set up the gating scheme (A) to identify all 5 populations (Mclass, Lclass, Bclass, Nclass, and Eclass) on a bivariate using the monocyte and basophil ML classifiers. Lymphocytes are negative for both ML classifiers, basophils are positive for the basophil ML classifier, and monocytes are positive for the monocyte ML classifier. As seen in Figure 6A, the neutrophil and eosinophil populations are both positive for the monocyte ML classifier and form clearly separated clusters, which allows us to resolve all 5 populations in a single plot. For comparison, Figure 6B shows the Mimm, Limm, Bimm, Nimm, and Eimm populations superimposed on the same plot. Note the excellent concordance between the populations identified by immunofluorescence (B) and those identified only using BF, SSC, and nuclear imagery (A), thereby demonstrating the efficacy of this approach.

classifier performance by applying it to multiple test samples. We evaluated more than 150 samples obtained from different donors on multiple ImageStream® instruments over several months. The first metric we evaluated was the relative percent of each of the five populations in the sample obtained by immunofluorescence compared to that obtained by the ML classifiers. To do this, we stained every one of the 150+ samples with specific markers (Panel 5-Part in Figure 1) to identify the five cell populations by immunofluorescence (Eimm, Nimm, Bimm, Mimm, and Limm), while also obtaining the five populations using the ML classifiers based only on BF, SSC, and nuclear imagery (Eclass, Nclass, Bclass, Mclass, and Lclass).

For every sample, we verified that the ML classified population percentages were consistent between the data from Panel 5-Part and Panel Test to ensure that there was no compensation bias. The results are shown in Figure 8A. As demonstrated, there is excellent sample-level correspondence between the immunofluorescence and the ML classification. The second metric we evaluated was the correctness of the ML classification results on a cell-by-cell basis. Using immunofluorescence as the gold standard, we evaluated the sensitivity and specificity of the ML classified populations using the formula shown in Figure 7. For the 150+ samples, we achieved on average more than 97% sensitivity and more than 99% specificity across all five cell types, with the breakdown for the individual cell types shown in Figure 8B. These results provide compelling evidence that our ML-based classification methodology using only the BF, SSC, and nuclear imagery can effectively identify populations without the need for specialized fluorescent markers.

	Classifier Positive	Classifier Negative
Immunofluorescence Positive	True Positives	False Negatives
Immunofluorescence Negative	False Positives	True Negatives

$$\text{Sensitivity} = \frac{\# \text{True Positives}}{\# \text{True Positives} + \# \text{False Negatives}}$$

$$\text{Specificity} = \frac{\# \text{True Negatives}}{\# \text{True Negatives} + \# \text{False Positives}}$$

Figure 7. Quantitative metrics to evaluate ML classification efficacy compared to immunofluorescence.

Conclusions

In this study, we described a classification method using ML to distinguish cells based on their appear-

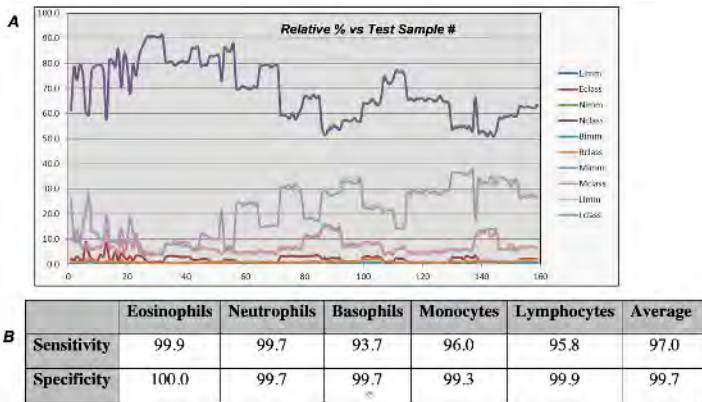


Figure 8. ML classifier efficacy assessment on 150+ test samples comparing the WBC five-part populations determined using immunofluorescence (Eimm, Nimm, Bimm, Mimm, and Limm, obtained using the gating scheme shown in Figure 2) to the WBC 5-part populations determined using the ML classifiers (Eclass, Nclass, Bclass, Mclass, and Lclass, obtained using the gating scheme shown in Figure 6). Figure 8A shows the relative proportions of each of the 5 populations determined by the two methods. The profiles match almost exactly in almost all cases. Figure 8B enumerates the degree of cell-cell concordance between the identified populations for the two methods. With all values over 95%, we can conclude that the populations resulting from the ML classification are equivalent to those obtained from immunofluorescence.

ance with parameter-rich image data collected on the Amnis ImageStream high-speed imaging flow cytometer. This approach is ideally suited to classification problems that do not lend themselves to single-parameter discrimination. The method, which is based on the LDA ML algorithm, combines multiple relevant and appropriately weighted discriminatory features into a single linear classifier that can be used to identify cells that exhibit characteristics similar to the corresponding hand-selected truth populations. Once a classifier is determined, it can be computed

and applied to all samples in similar experiments.

We also demonstrated the application of the ML classification method to perform five-part differential analysis in WBCs without the use of immunofluorescence. We showed that by intelligently combining key image morphology characteristics, we can obtain results equivalent to what is obtained with immunofluorescence—both at a sample and an individual cell level—without the time and expense of needing to stain samples with multiple markers. In addition to these benefits, our results demonstrate that this classification method is effective for applications where population detection by immunofluorescence is either not possible or is impractical.

The ability of the computed ML classifiers to generalize across multiple experiments, instruments, and time points is influenced by the quality of the input training data and discriminatory parameters chosen. Through the WBC five-part differential example, we have shown that with appropriate training sets and image features that are known to be robust to expected variations, this method can generate highly efficacious and robust classifiers. We believe that the ML-based classification framework described here for providing objective, multi-parametric statistical analysis of large data sets will serve as a powerful tool for finding targeted cell populations in samples for a diverse range of applications.

About the authors

Both authors are employees of Luminex Corporation. Vidya Venkatachalam, Ph.D., is the Senior Director for Software and Algorithms R&D for Flow Cytometry and Phil Morrissey, Ph.D., is a Senior Scientist.

For Research Use Only. Not for use in diagnostic procedures.

Amnis, ImageStream, and IDEAS are trademarks of Luminex Corporation, and are registered in the U.S. and other countries.



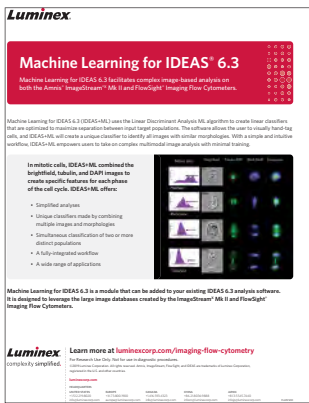
Resources



Amnis® ImageStream® Mk II



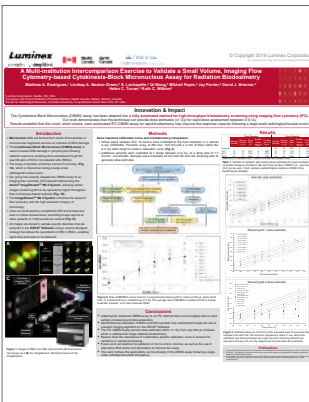
Amnis® FlowSight



Machine Learning for IDEAS® 6.3



Amnis® AI Image Analysis Software



A Multi-institution Intercomparison Exercise to Validate a Small Volume, Imaging Flow Cytometry-based Cytokinesis-Block Micronucleus Assay for Radiation Biodosimetry



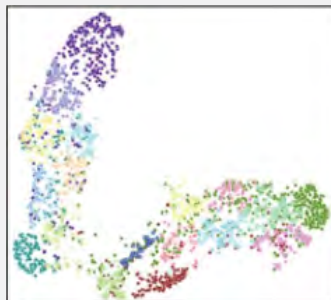
Luminex

Amnis[®] AI

Image Analysis Software for the ImageStream[®]X Mk II
and FlowSight[®] Imaging Flow Cytometers

A new frontier in image analysis: High-throughput image cytometry meets the power of artificial intelligence.

Object Map



Discover new phenotypes:

The object map characterizes unique populations using high-dimensional data reduction algorithms.

Confusion Matrix

	99	1	0	0
True	0	96	4	0
	0	2	98	0
	0	0	1	99

Predicted Class

Monitor AI performance:

The confusion matrix demonstrates how accurately the AI matched user-derived ground truth.

Harness the power of artificial intelligence, which supports:

- Computer-aided hand-tagging
- Clustering with object map plots
- Accuracy analytics and confusion matrix generation
- Deep learning AI model using convolutional neural networks (CNNs)

Luminex[®]
complexity simplified.

luminexcorp.com

For more information on what Amnis[®] AI can do, please visit:
luminexcorp.com/imagestreamx-mk-ii/#software.

For Research Use Only. Not for use in diagnostic procedures.

©2020 Amnis, ImageStream, and FlowSight are trademarks of Luminex Corporation, registered in the US and other countries.

DIGI274495